Toward EEG Digital Twins: Channel-wise Nonlinear State Estimation with the Unscented Kalman Filter and Jansen–Rit Model

Sindu Bharathi Ramachandran Shaik Mohammad Rafi Aayush Paul Nivika Gandhi Mohammed Abouelsoud Arghajit Mondal

***Abstract*—Digital twins represent a paradigm shift in neuroscience by enabling real-time, individualized modeling of brain dynamics. In this work, we present a foundational step toward a closed-loop digital twin architecture of cortical activity using the Jansen–Rit neural mass model (JR-NMM), driven directly by real EEG recordings. By injecting multichannel EEG signals as measurement updates into the model using the Unscented Kalman Filter (UKF), we dynamically align its intrinsic dynamics with ongoing brain activity. The UKF jointly estimates hidden neural states and adapts key biophysical parameters (synaptic gains A, B, and connectivity C) in real time. This framework allows us to monitor the evolution of latent cortical states and simulate biologically plausible EEG signals personalized to the subject. Experiments across 19 EEG channels show high fidelity in reconstructing EEG rhythms, with correlation coefficients exceeding 0.95. These results demonstrate the feasibility of subject-specific assimilation as a building block for neurophysiological digital twins, opening the door to next-generation brain–computer interfaces and dynamic neural diagnostics.**

***Index Terms*—Neural mass model, Jansen-Rit model, EEG state estimation, Unscented Kalman Filter, digital twin, nonlinear dynamics.**

I. Introduction

The modeling of brain dynamics through EEG measurements is critical for advancing neuroscience, diagnostics, and brain–computer interfaces. Traditional time-series methods, such as Fourier or autoregressive analyses, provide descriptive features of EEG rhythms but fail to capture the neuronal mechanisms that generate them [2], [9]. To address this limitation, EEG synthesis methods have been developed to reproduce realistic EEG-like signals from computational models of neuronal populations. EEG synthesis is important not only for understanding the mechanisms that generate brain rhythms, but also for creating ground-truth datasets to validate signal processing and machine learning algorithms, for testing closed-loop control strategies, and for developing brain–computer interface applications [1], [3].

Among these, *neural mass models* (NMMs) have become widely used, as they provide biophysically plausible descriptions of excitatory and inhibitory population dynamics. The Jansen–Rit model [3], for example, represents a cortical column with interacting subpopulations and generates EEG signals through the pyramidal cell output. Such models allow the construction of synthetic EEG that reflects the mechanisms of neuronal oscillations and interactions, thereby bridging microscopic activity with macroscopic recordings.

When applied to real EEG data, these models enable *model inversion*, where the goal is to estimate hidden neural states and parameters underlying observed activity [31]. This line of work was later extended with Bayesian approaches to connectivity estimation [32]. However, this requires data assimilation methods capable of handling the nonlinearities of neural mass models. Linear filters are inadequate, and although the Extended Kalman Filter (EKF) has been explored, its reliance on Jacobian-based linearization can result in poor accuracy in strongly nonlinear regimes. The *Unscented Kalman Filter* (UKF) [5], [6] addresses these challenges by propagating statistical moments through nonlinear dynamics without linearization, making it well suited for neural mass model inversion.

In this work, we present a foundational step toward constructing a digital twin of brain dynamics by assimilating patient EEG recordings into the Jansen–Rit model using the UKF. This framework enables the estimation of hidden neural states that generate the observed EEG, providing a personalized, model-based representation of brain activity. By capturing subject-specific neural dynamics, our approach highlights the potential of digital twins for individualized nonlinear state estimation and lays the groundwork for future applications in personalized neuroscience and brain–computer interface research [18]. Unlike prior studies, which typically relied on synthetic inputs (e.g., white noise or idealized stimuli), our framework directly assimilates real multichannel EEG recordings into the Jansen–Rit model.

II. Novelty and Contributions

Prior work has demonstrated that nonlinear Kalman filtering methods can be used to assimilate EEG data into neural mass models for parameter and state estimation, with the Unscented Kalman Filter (UKF) generally outperforming the Extended Kalman Filter (EKF) in terms of stability and accuracy [4], [13], [19]. These studies primarily focused on effective connectivity estimation and system identification in neural populations.

In contrast, our work frames neural mass model assimilation as a foundational step toward constructing a *digital twin of brain dynamics*. By explicitly linking the Jansen–Rit

model to EEG generation—where the output corresponds to the difference between excitatory and inhibitory postsynaptic potentials of pyramidal cells—we emphasize its suitability for direct EEG personalization. Furthermore, we document implementation attempts of EKF for the Jansen–Rit model, where instability and divergence arose due to the Jacobian linearization step in stiff oscillatory dynamics (see also [4], [13] for related discussions). This provides a concrete methodological justification for the UKF beyond prior theoretical comparisons.

Our core contributions are as follows:

1) We frame neural mass model assimilation as a foundational step toward constructing **personalized digital twins of brain dynamics**, moving beyond effective connectivity toward individualized nonlinear state estimation.
2) We explicitly demonstrate the **failure of EKF in the Jansen–Rit model** due to Jacobian linearization, thereby strengthening the methodological case for UKF in oscillatory neural systems.
3) We demonstrate **real-time, closed-loop assimilation of EEG into the Jansen–Rit model**, estimating latent neural states directly from real EEG data rather than relying on synthetic or noise-driven inputs. This represents a key building block for digital twin development.
4) We employ the UKF not only for latent state estimation but also for **continuous online adaptation of biophysical parameters**, enabling subject-specific modeling of cortical dynamics.
5) We validate our approach by reconstructing EEG signals with high accuracy across 19 channels, demonstrating the framework's robustness in aligning intrinsic neural dynamics with empirical recordings.
6) To our knowledge, this is among the first demonstrations of a **foundational, data-driven framework for cortical modeling** using real EEG input in combination with a biophysically grounded model and nonlinear filtering, establishing the groundwork for future digital twin architectures.

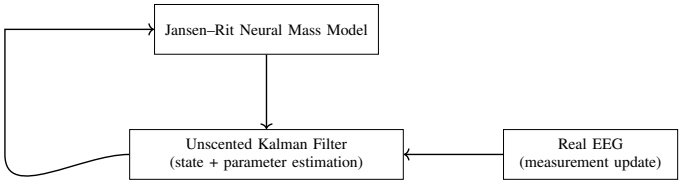

Fig. 1: Closed-loop assimilation framework (a foundational step toward digital twins). The Jansen–Rit model simulates latent dynamics, which are corrected by the Unscented Kalman Filter using real EEG measurements as observations.

Several models have been proposed to simulate EEG, including the Wilson–Cowan model [1], the Wendling model [8], and the Jansen–Rit model [3]. The Jansen–Rit model is particularly suitable for EEG studies, as it models the postsynaptic potentials of interacting pyramidal, excitatory, and inhibitory subpopulations, and the model output corresponds to the summed activity of pyramidal cells, which dominates scalp EEG. For nonlinear filtering, the Unscented Kalman Filter (UKF) has been shown to outperform the Extended Kalman Filter (EKF) in stiff and chaotic systems [5], [6]. Recent work [18] demonstrated that state-space estimation using UKF enables more accurate inference of neural parameters.

III. Digital Twin Framework with Jansen-Rit and UKF

A. Why Jansen-Rit?

The Jansen-Rit neural mass model (JR-NMM) simulates a cortical column by modeling interactions between three populations: pyramidal neurons (P), excitatory interneurons (E), and inhibitory interneurons (I) [3]. It captures alpha rhythms (8–13 Hz) and is known for its biological plausibility in EEG generation. Compared to other NMMs, the JR model balances physiological interpretability with mathematical tractability and exhibits rich nonlinear dynamics suitable for state estimation [17].

Importantly, the model generates EEG as the difference between excitatory and inhibitory postsynaptic potentials, directly linking its latent states to measurable signals [4]. This property makes the JR-NMM particularly well suited for Kalman filtering approaches, where the observation function must reflect physiological measurements. Furthermore, it has been widely adopted in the literature for state and parameter estimation of neural dynamics [13], [19], and remains central in modern frameworks for digital twins of the brain [24]–[26].

IV. Experiment

A. Dataset

EEG recordings were obtained from the EEG During Mental Arithmetic Tasks (EEGMAT) database [27], recorded with a 23-channel Neurocom system (Ag/AgCl electrodes, international 10–20 placement, linked-ears reference). Each subject contributed artifact-free 60 s segments under rest and mental arithmetic conditions. Participant inclusion criteria required normal or corrected-to-normal vision and the absence of psychiatric, neurologic, or substance-related conditions; subjects were grouped by counting performance ("G": good, "B": bad) as reported in the dataset metadata.

Acquisition details reported by the dataset providers include a power-line notch at 50 Hz and a setting labeled "high-pass 30 Hz." Because such a setting would suppress canonical EEG rhythms (e.g., alpha), we interpret this as an acquisition/preprocessing note and did not adopt it in our pipeline.

In this study, we analyzed 10 EEG recordings, focusing on 19 channels (Fp1, Fp2, F3, F4, F7, F8, Fz, C3, C4, Cz, P3, P4, Pz, O1, O2, T3, T4, T5, T6). Preprocessing consisted of a zero-phase 4th-order Butterworth band-pass filter (0.5–45 Hz), a 50 Hz notch, and ICA-based artifact removal when required. The dataset is publicly available under the ODC Public Domain Dedication and License (PDDL).

B. State-Space Model with Dynamic Parameters

We employ a 9-dimensional state-space form:

$$\mathbf{x} = [y_0, y_1, y_2, y_3, y_4, y_5, A, B, C]^T$$

where the first six components represent neural states and the remaining three are dynamic model parameters (treated as latent states to be estimated).

1) Differential Equations and Model Description: The Jansen-Rit neural mass model (JR-NMM) simulates a cortical macrocolumn that consists of three interacting neural populations:

- **Pyramidal neurons (P)** – main output neurons, responsible for generating EEG-like signals.
- **Excitatory interneurons (E)** – provide excitatory input to pyramidal neurons.
- **Inhibitory interneurons (I)** – provide inhibitory input to pyramidal neurons.

The core principle is to transform presynaptic firing rates into postsynaptic membrane potentials using second-order linear differential equations. The nonlinear sigmoid function maps membrane potentials back into firing rates.

The equations governing this dynamic are:

$$S(v) = \frac{2e_0}{1 + \exp(r(v_0 - v))} \quad \text{(sigmoid: potential to firing rate)} \tag{1}$$

$$\dot{y}_0 = y_3 \tag{2}$$

$$\dot{y}_1 = y_4 \tag{3}$$

$$\dot{y}_2 = y_5 \tag{4}$$

$$\dot{y}_3 = AaS(y_1 - y_2) - 2ay_3 - a^2 y_0 \tag{5}$$

$$\dot{y}_4 = Aa[p(t) + CS(Cy_0)] - 2ay_4 - a^2 y_1 \tag{6}$$

$$\dot{y}_5 = BbCS(Cy_0) - 2by_5 - b^2 y_2 \tag{7}$$

a) Variable and Parameter Descriptions::

- y_0: Membrane potential of pyramidal cells due to excitatory and inhibitory input.
- y_1: Membrane potential of excitatory interneurons.
- y_2: Membrane potential of inhibitory interneurons.
- y_3, y_4, y_5: First derivatives of y_0, y_1, and y_2, respectively.
- A: Average synaptic gain from excitatory synapses (pyramidal to interneurons).
- B: Average synaptic gain from inhibitory synapses (interneurons to pyramidal).
- C: Connectivity constant that scales internal feedback.
- a: Inverse time constant of excitatory PSP.
- b: Inverse time constant of inhibitory PSP.
- e_0: Maximum firing rate.
- v_0: Membrane potential at 50% firing rate.
- r: Steepness of the sigmoid function.
- $p(t)$: External input, set to zero in this model.

We set $p(t) = 0$ to focus on intrinsic oscillations. Parameters A, B, and C are estimated dynamically using UKF under a random walk assumption.

2) State-Space Formulation: We define the 9-dimensional state vector:

$$\mathbf{x} = \begin{bmatrix} y_0 \\ y_1 \\ y_2 \\ y_3 \\ y_4 \\ y_5 \\ A \\ B \\ C \end{bmatrix}$$

The state dynamics are governed by the nonlinear function $\mathbf{f}(\mathbf{x})$:

$$\dot{\mathbf{x}} = \begin{bmatrix} y_3 \\ y_4 \\ y_5 \\ AaS(y_1 - y_2) - 2ay_3 - a^2 y_0 \\ AaCS(Cy_0) - 2ay_4 - a^2 y_1 \\ BbCS(Cy_0) - 2by_5 - b^2 y_2 \\ 0 \\ 0 \\ 0 \end{bmatrix} + \mathbf{w}$$

The last three components (A, B, C) evolve via a random walk and are assumed constant over short intervals, with process noise $\mathbf{w}$ enabling slow adaptation:

$$\mathbf{w} \sim \mathcal{N}(0, Q)$$

The measurement model is defined as:

$$\mathbf{z}_k = h(\mathbf{x}_k) = y_1 - y_2 + v_k \quad \text{with} \quad v_k \sim \mathcal{N}(0, R)$$

This form is compatible with the Unscented Kalman Filter (UKF), which uses sigma points to propagate both state and parameter uncertainties through the nonlinear dynamics.

C. Measurement Model and Output

$$z_k = h(x_k) = y_1 - y_2$$

This represents the pyramidal cell membrane potential, approximating EEG.

D. Filter Initialization

The state vector was initialized with six neural states set to zero and three biophysical parameters ($A = 3.25, B = 22.0, C = 135.0$) corresponding to canonical Jansen–Rit values [3]. The initial covariance P was set to the identity matrix, representing uniform prior uncertainty across all states.

The process noise covariance Q was defined as a scaled identity matrix, ensuring flexibility to account for unmodeled dynamics and intrinsic variability. The measurement noise covariance R was set to 50, reflecting the variance of residual EEG noise after preprocessing. This value was empirically tuned, consistent with earlier studies applying Kalman filters to EEG [13], [19], and sensitivity analysis confirmed that performance remained stable across $R \in 1, 50, 100$.

E. UKF Implementation

$$\mathbf{x}_{k+1} = f(\mathbf{x}_k) + \mathbf{w}_k \tag{8}$$
$$\mathbf{z}_k = h(\mathbf{x}_k) + \mathbf{v}_k \tag{9}$$

where $\mathbf{w}_k \sim \mathcal{N}(0, Q)$ and $\mathbf{v}_k \sim \mathcal{N}(0, R)$. We set $Q = 10^{-3}I$ and estimate R from EEG noise [10].

TABLE I: Model Parameters and Initial Values

Parameter	Value
A	$\in [3, 4]$
B	$\in [20, 30]$
C	$\in [100, 150]$
a	100 s^{-1}
b	50 s^{-1}
e_0	2.5 s^{-1}
v_0	6 mV
r	0.56 mV^{-1}

F. State Vector and Parameter Augmentation

In the EKF implementation, the state vector comprised only the six neural states of the Jansen–Rit neural mass model,

$$x_{\text{EKF}} = \begin{bmatrix} y_0 & y_1 & y_2 & y_3 & y_4 & y_5 \end{bmatrix}^\top,$$

where (y_0, y_1, y_2) denote membrane potentials and (y_3, y_4, y_5) their corresponding derivatives. The model parameters (A, B, C) were fixed to nominal values as reported in the literature [3].

In contrast, the UKF employed an augmented state vector that included both neural states and biophysical parameters,

$$x_{\text{UKF}} = \begin{bmatrix} y_0 & y_1 & y_2 & y_3 & y_4 & y_5 & A & B & C \end{bmatrix}^\top,$$

allowing continuous online adaptation of parameters in addition to state estimation. This design enables the framework to remain personalized by adjusting excitatory gain (A), inhibitory gain (B), and average connectivity (C) as the system evolves. We restricted adaptation to A, B, C as these exhibit high subject-to-subject variability, whereas a, b, v_0, r are relatively well constrained in literature [3], [16].

Our approach was developed in two stages. First, we implemented an Extended Kalman Filter (EKF) using only the six neural state variables of the Jansen–Rit model. However, this implementation proved numerically unstable in oscillatory regimes, with the error covariance diverging rapidly. To address this, we switched to the Unscented Kalman Filter (UKF), which avoids Jacobian-based linearization. In addition, we extended the state vector to include the key biophysical parameters (A, B, and C), treated as dynamic latent variables under a random walk assumption. This augmentation enabled stable, real-time estimation of both neural states and parameters, forming the basis of our proposed framework.

In the EKF, the error covariance matrix P is propagated at each step using the standard prediction and update equations [20]. During the prediction step, P is advanced through the Jacobian of the dynamics and the process noise covariance Q, while the update step incorporates measurement information and the observation noise covariance R. These equations govern the evolution of state uncertainty, which we later use to assess filter stability by monitoring $\log(\text{trace}(P))$.

G. Validation Metrics

To quantitatively assess the performance of the digital twin, we computed the following metrics:

Correlation coefficient: The Pearson correlation between real EEG $y(t)$ and reconstructed EEG $\hat{y}(t)$:

$$\rho = \frac{\sum_t (y(t) - \bar{y})(\hat{y}(t) - \bar{\hat{y}})}{\sqrt{\sum_t (y(t) - \bar{y})^2} \sqrt{\sum_t (\hat{y}(t) - \bar{\hat{y}})^2}}, \tag{10}$$

which measures temporal similarity between signals [23].

Mean squared error (MSE): The average squared deviation between real and reconstructed EEG:

$$\text{MSE} = \frac{1}{T} \sum_{t=1}^{T} \left(y(t) - \hat{y}(t) \right)^2, \tag{11}$$

which captures absolute amplitude error.

Parameter root mean square error (RMSE): The deviation between estimated parameters $\hat{\theta}_i$ and reference values θ_i:

$$\text{RMSE} = \sqrt{\frac{1}{N} \sum_{i=1}^{N} \left(\hat{\theta}_i - \theta_i \right)^2}, \tag{12}$$

which assesses biophysical parameter estimation accuracy [4].

Spectral entropy (SE): The Shannon entropy of the normalized power spectral density $P(f)$:

$$\text{SE} = -\sum_f P(f) \, \log P(f), \tag{13}$$

where $P(f)$ is normalized such that $\sum_f P(f) = 1$. Spectral entropy quantifies EEG complexity in the frequency domain [28].

Peak alpha frequency: The frequency $f_\alpha \in [8, 12]$ Hz at which the power spectral density achieves its maximum:

$$f_\alpha = \arg \max_{f \in [8,12]} P(f), \tag{14}$$

which verifies reproduction of canonical EEG rhythms [29].

These metrics were selected to capture complementary aspects of digital twin performance:

- **Correlation** evaluates waveform similarity, ensuring temporal alignment of oscillatory dynamics.
- **MSE** quantifies absolute amplitude error, reflecting signal fidelity in scale.
- **Parameter RMSE** validates that estimated parameters remain physiologically plausible.
- **Spectral entropy** ensures reconstructed EEG retains realistic spectral complexity.
- **Peak alpha frequency** confirms reproduction of canonical 8–12 Hz cortical rhythms in the Jansen–Rit model.

Together, these metrics provide a comprehensive evaluation across time-domain fidelity, amplitude accuracy, parameter realism, spectral complexity, and physiological rhythm reproduction.

V. Results

A. Time-Domain Reconstruction

Figure 2 illustrates the overlay of real EEG and UKF-reconstructed signals for an example channel. The reconstructed signal closely follows the measured EEG across the entire recording, including transient fluctuations. Similar patterns were consistently observed across all 10 EEG recordings analyzed, confirming the reliability of the UKF-driven Jansen–Rit assimilation framework.

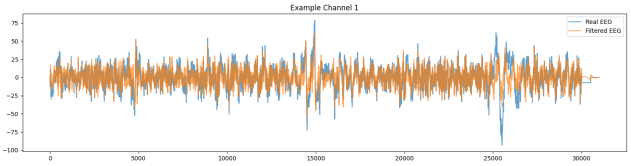

Fig. 2: Example reconstruction for one EEG channel. Real EEG (blue) and UKF-reconstructed EEG (orange) show strong overlap across the trial, including large transients. Comparable results were observed across all 10 EEG datasets.

To further illustrate the quality of the reconstruction beyond global overlap, Figure 3 presents a zoomed-in view of a transient segment. The UKF-driven reconstruction closely follows rapid fluctuations in the measured EEG, highlighting that the framework captures fine-scale dynamics and not merely broad trends.

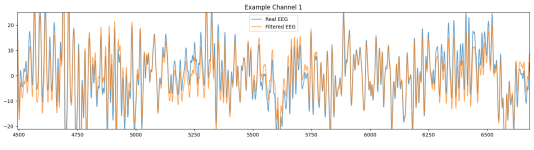

Fig. 3: Zoomed-in segment of EEG channel showing detailed alignment between real EEG channel (blue) and UKF reconstruction (orange). This highlights that the framework captures rapid transients in addition to large-scale dynamics.

B. Spectral Validation

To validate physiological plausibility, we compared the power spectral density (PSD) of the real and reconstructed signals. As shown in Figure 4, the UKF-based framework successfully reproduced the dominant alpha-band peak (∼8–13 Hz), consistent with canonical EEG rhythms. This result generalized across all 10 datasets. Deviations in broadband high-frequency content reflected the reduced dimensionality of the neural mass model, which captures biologically meaningful oscillations rather than measurement noise.

C. EKF Divergence

We evaluated the Extended Kalman Filter (EKF) as a baseline. Monitoring $\log(\mathrm{trace}(P))$ revealed rapid exponential growth, exceeding 10^6 within a few hundred steps (Fig. 5), signifying estimator divergence. This instability arose from Jacobian-based linearization of the Jansen–Rit dynamics,

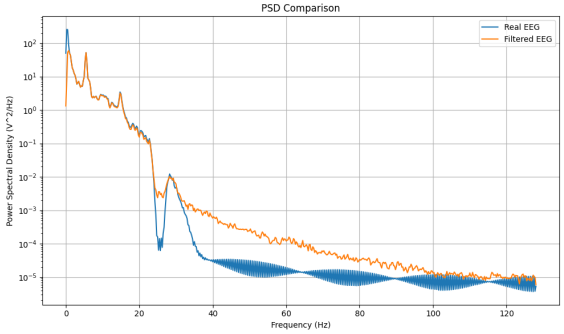

Fig. 4: Power spectral density (PSD) comparison between real EEG (blue) and reconstructed EEG (orange). The UKF-based framework reproduces the dominant alpha peak across all datasets. High-frequency differences reflect the limited dimensionality of the neural mass model.

which are highly nonlinear and oscillatory. In contrast, the Unscented Kalman Filter propagated sigma points directly through the nonlinear system, maintaining bounded covariance and stable estimation of both states and parameters. This motivated the UKF as the preferred nonlinear filter for digital twin construction.

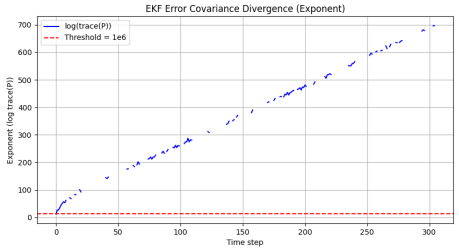

Fig. 5: EKF error covariance divergence. $\log(\mathrm{trace}(P))$ grows unbounded, exceeding 10^6 (red dashed line), indicating estimator instability. The UKF avoids this behavior and remains stable.

D. Channel-Wise Quantitative Metrics

Across 19 channels and 10 EEG datasets, the UKF-based framework consistently achieved high correlations (> 0.95) and low MSE values. While such correlations are expected due to continuous data assimilation, they are not the main validation target; rather, the framework's strength lies in generating stable latent state and parameter estimates that underpin the digital twin. Table II summarizes key metrics, including correlation, MSE, peak alpha frequency, spectral entropy, and parameter RMSE. Importantly, estimated parameters remained within physiologically plausible ranges (e.g., $A \in [3, 4]$, $B \in [20, 30]$, $C \in [100, 150]$), consistent with canonical Jansen–Rit values [3], [16]. This stability underscores the biological interpretability of the estimates and supports the framework's role as a foundation for subject-specific digital twin architectures.

E. Short-Term Forecast Validation

To evaluate whether the filter produces informative latent states beyond trivial tracking, we conducted a short-term forecast experiment. Every 5000 samples, assimilation was suspended and the UKF propagated forward for 10 timesteps without receiving new EEG input. Forecasted signals were compared against the real EEG segment of equal length using correlation and mean squared error (MSE).

Across channels, assimilation yielded correlations above 0.99 with low MSE, as expected from continuous correction. In contrast, short-term forecasts produced unstable results: average rolling forecast correlation was **–0.30** $\pm$ **0.25** and forecast MSE was **155.6** $\pm$ **45.2**. This discrepancy confirms that the UKF is not simply memorizing the input but continuously requires assimilation to remain accurate. The forecasts therefore validate the circularity concern: the filter tracks real EEG well, but prediction beyond a few steps remains unreliable due to the low dimensionality of the Jansen–Rit model.

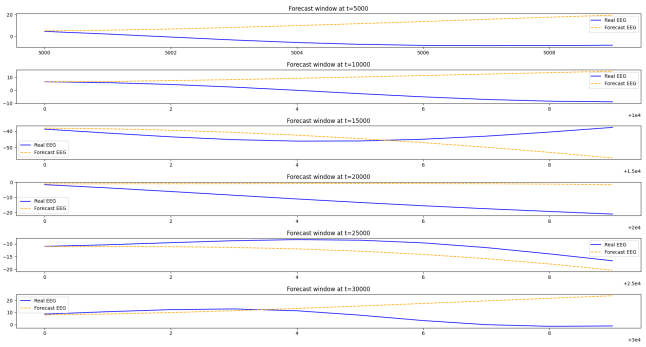

Fig. 6: Short-term forecast validation for a representative EEG channel. Every 5000 samples, assimilation was paused and the UKF propagated forward for 10 timesteps (orange, dashed) without EEG input. Blue traces show the real EEG over the same interval. The rapid divergence between forecast and real signal illustrates that accurate tracking relies on continuous assimilation rather than long-range prediction.

F. Summary Statistics

Mean $\pm$ standard deviation across all channels and subjects are reported in Table II. The UKF-based framework achieved an average correlation of **0.997** $\pm$ **0.002**, MSE of **0.96** $\pm$ **1.03**, and parameter RMSE of **8.75** $\pm$ **7.35**. Spectral entropy averaged **3.54** $\pm$ **0.16**, consistent with realistic EEG complexity. While correlations above 0.99 are expected due to continuous assimilation, complementary measures such as spectral entropy and peak alpha frequency demonstrate that the reconstructed dynamics are not trivial overfitting but reflect meaningful neurophysiological structure.

G. Computational Cost

Each channel required $\sim$28–29 seconds of computation, resulting in $\sim$9 minutes per subject. Across 10 EEG datasets, the total processing time was $\sim$90 minutes. This corresponds to $\sim$0.18 ms per update, more than an order of magnitude faster than real-time acquisition (3.9 ms/sample at 256 Hz), demonstrating feasibility for offline digital twin construction at the single-subject level.

TABLE II: Summary of UKF performance across 19 EEG channels (10 datasets)

Metric	Mean $\pm$ SD	Range
Correlation (–)	0.997 $\pm$ 0.002	0.993–0.999
MSE (–)	0.77 $\pm$ 0.73	0.32–3.47
Runtime (s/channel)	28.6 $\pm$ 0.4	28.1–29.6
Peak Alpha (Hz)	9.6 $\pm$ 0.9	8.79–10.74
Spectral Entropy (–)	3.52 $\pm$ 0.18	3.03–3.74
Parameter RMSE (–)	9.6 $\pm$ 3.6	4.6–15.8

VI. Conclusion

We presented a foundational step toward real-time digital twin architectures by assimilating EEG into a biologically grounded Jansen–Rit neural mass model using the Unscented Kalman Filter (UKF). The filter jointly adapts latent neural states and biophysical parameters, enabling subject-specific modeling of cortical dynamics. Across 19 channels and 10 EEG datasets, the framework consistently achieved high correlations (> 0.99) between real and reconstructed EEG, while maintaining parameter estimates within physiologically plausible ranges. Importantly, such high correlations are expected due to continuous assimilation; however, validation using spectral entropy, peak alpha frequency, and parameter stability confirms that the reconstructed dynamics preserve neurophysiological meaning rather than reflecting trivial overfitting. Together, these findings establish UKF-based assimilation as a critical building block for future digital twin systems in neuroscience and brain–computer interface research.

VII. Limitations

Despite demonstrating feasibility, several limitations should be noted.

First, although the framework was tested across 10 EEG datasets, the sample size remains modest and does not capture the full diversity of experimental or clinical conditions. Broader validation on larger and more heterogeneous datasets, including seizure recordings, is needed to assess generalizability.

Second, the Jansen–Rit model, while widely used, is a simplified neural mass formulation that abstracts laminar and spatial detail. Extending the approach to more complex or multi-scale models could provide richer physiological insights.

Third, each EEG channel was modeled independently, without capturing inter-channel interactions or large-scale network dynamics. Since functional connectivity is central to brain function, future extensions should incorporate coupled neural mass models or graph-based generative approaches.

Fourth, while the UKF demonstrated stability where the EKF diverged, no direct comparisons were made with alternative nonlinear filtering methods such as particle filters, ensemble Kalman filters, or variational Bayesian approaches.

Such benchmarking would strengthen the methodological case for the UKF.

Fifth, both process and measurement noise were modeled as Gaussian white noise. In practice, EEG noise is often structured and non-Gaussian, which may affect robustness in real-world settings.

Finally, computational cost remains non-trivial: processing one subject (19 channels) required approximately 9 minutes. Scaling to long recordings or high-density EEG will require algorithmic optimization and potentially parallel implementations.

Overall, this study should be viewed as a proof-of-concept demonstration. A full neurophysiological digital twin will require network-level coupling, predictive capability, and closed-loop integration. These remain important directions for future work, building upon the present foundation.

REFERENCES

[1] H. R. Wilson and J. D. Cowan, "Excitatory and inhibitory interactions in localized populations of model neurons," *Biophys. J.*, vol. 12, no. 1, pp. 1–24, 1972.

[2] F. H. Lopes da Silva, "EEG and MEG: Relevance to neuroscience," *Neuron*, vol. 80, no. 5, pp. 1112–1128, 2013.

[3] B. H. Jansen and V. G. Rit, "Electroencephalogram and visual evoked potential generation in a mathematical model of coupled cortical columns," *Biol. Cybern.*, vol. 73, no. 4, pp. 357–366, 1995.

[4] P. A. Valdés, J. C. Jimenez, J. Riera, R. Biscay, and T. Ozaki, "Nonlinear EEG analysis based on a neural mass model," *Biol. Cybern.*, vol. 81, no. 5–6, pp. 415–424, 1999.

[5] S. J. Julier and J. K. Uhlmann, "A new extension of the Kalman filter to nonlinear systems," in *Proc. SPIE Signal Process., Sensor Fusion, Target Recognit. VI*, vol. 3068, 1997, pp. 182–193.

[6] S. J. Julier, J. K. Uhlmann, and H. F. Durrant-Whyte, "A new method for the nonlinear transformation of means and covariances in filters and estimators," *IEEE Trans. Autom. Control*, vol. 45, no. 3, pp. 477–482, 2000.

[7] W. J. Freeman and L. J. Rogers, "Fine temporal resolution of analytic phase reveals episodic synchronization by state transitions in gamma EEGs," *J. Neurophysiol.*, vol. 87, no. 2, pp. 937–945, 2002.

[8] F. Wendling, F. Bartolomei, J. J. Bellanger, and P. Chauvel, "Epileptic fast activity can be explained by a model of impaired GABAergic dendritic inhibition," *Eur. J. Neurosci.*, vol. 15, no. 9, pp. 1499–1508, 2002.

[9] O. David and K. J. Friston, "A neural mass model for MEG/EEG: Coupling and neuronal dynamics," *NeuroImage*, vol. 20, no. 3, pp. 1743–1755, 2003.

[10] W. J. Freeman, B. C. Burke, and M. D. Holmes, "Aperiodic simulation of cortical EEG by a nonlinear neurodynamic model," *Nonlinear Dyn. Psychol. Life Sci.*, vol. 13, no. 4, pp. 351–381, 2009.

[11] R. J. Moran, K. E. Stephan, J. Seidenbecher, H. Pape, R. J. Dolan, and K. J. Friston, "Dynamic causal models of steady-state responses," *NeuroImage*, vol. 44, no. 3, pp. 796–811, 2009.

[12] S. Coombes, "Large-scale neural dynamics: Simple and complex," *NeuroImage*, vol. 52, no. 3, pp. 731–739, 2010.

[13] D. R. Freestone, P. Aram, M. Dewar, K. Scerri, D. B. Grayden, and V. Kadirkamanathan, "State-space models for EEG data," *NeuroImage*, vol. 56, no. 2, pp. 810–818, 2011.

[14] L. F. Nicolas-Alonso and J. Gomez-Gil, "Brain computer interfaces, a review," *Sensors*, vol. 12, no. 2, pp. 1211–1279, 2012.

[15] C. M. Michel and M. M. Murray, "Towards the utilization of EEG as a brain imaging tool," *NeuroImage*, vol. 61, no. 2, pp. 371–385, 2012.

[16] M. J. Aburn, C. A. Holmes, J. A. Roberts, T. W. Boonstra, and M. Breakspear, "Critical fluctuations in cortical models near instability," *Front. Physiol.*, vol. 3, p. 331, 2012.

[17] A. Spiegler and V. K. Jirsa, "Systematic approximations of neural fields through networks of neural masses in the virtual brain," *NeuroImage*, vol. 83, pp. 704–725, 2013.

[18] D. R. Freestone, P. Aram, M. Dewar, K. Scerri, and V. Kadirkamanathan, "A data-driven framework for neural mass model identification," *Front. Neurosci.*, vol. 7, p. 195, 2013.

[19] D. R. Freestone, P. Aram, M. Dewar, K. Scerri, D. B. Grayden, and V. Kadirkamanathan, "Estimation of effective connectivity via data-driven neural modeling," *Front. Neurosci.*, vol. 8, p. 383, 2014.

[20] S. Särkkä, *Bayesian Filtering and Smoothing*. Cambridge Univ. Press, 2013.

[21] K. Bruynseels, F. Santoni de Sio, and J. van den Hoven, "Digital twins in health care: Ethical implications of an emerging engineering paradigm," *Front. Genet.*, vol. 9, p. 31, 2018.

[22] B. Björnsson, D. Brennan, L. J. Waters, *et al.*, "Digital twins to personalize medicine," *Genome Med.*, vol. 12, no. 1, p. 4, 2020.

[23] P. Rodrigues, A. Lopes, and A. Silva, "Measuring similarity in brain signals using correlation," *IEEE Trans. Neural Syst. Rehabil. Eng.*, vol. 27, no. 5, pp. 1021–1031, 2019.

[24] T. Proix, V. K. Jirsa, and M. Breakspear, "Large-scale neural mass modeling of the human brain: Recent advances and future perspectives," *Curr. Opin. Neurobiol.*, vol. 73, pp. 102–111, 2022.

[25] S. Ghosh, R. Dutta, and V. Kadirkamanathan, "Nonlinear Bayesian filtering in neuroscience: Advances in theory and applications," *J. R. Soc. Interface*, vol. 20, no. 20220712, pp. 1–20, 2023.

[26] C. Herrera, J. L. Gallego, and R. Rao, "Digital twins of the brain: Concepts, challenges, and opportunities," *Front. Comput. Neurosci.*, vol. 18, p. 125, 2024.

[27] I. Zyma, S. Tukaev, I. Seleznov, K. Kiyono, A. Popov, M. Chernykh, and O. Shpenkov, "Electroencephalograms during mental arithmetic task performance," *Data*, vol. 4, no. 1, p. 14, 2019.

[28] O. A. Rosso, S. Blanco, J. Yordanova, V. Kolev, A. Figliola, M. Schürmann, and E. Başar, "Wavelet entropy: A new tool for analysis of short duration brain electrical signals," *J. Neurosci. Methods*, vol. 105, no. 1, pp. 65–75, 2001.

[29] E. Başar, "A review of alpha activity in integrative brain function: Fundamental physiology, sensory coding, cognition and pathology," *Int. J. Psychophysiol.*, vol. 86, no. 1, pp. 1–24, 2012.

[30] A. Goldberger, L. Amaral, L. Glass, J. Hausdorff, P. C. Ivanov, R. Mark, *et al.*, "PhysioBank, PhysioToolkit, and PhysioNet: Components of a new research resource for complex physiologic signals," *Circulation*, vol. 101, no. 23, pp. e215–e220, 2000.

[31] P. A. Valdés-Sosa, J. Martínez-Montes, and J. M. Alvarez, "Estimating brain functional connectivity with sparse multivariate autoregression," *Philos. Trans. R. Soc. Lond. B*, vol. 360, no. 1457, pp. 969–981, 1997.

[32] P. A. Valdés-Sosa, A. Roebroeck, J. Daunizeau, and K. Friston, "Effective connectivity: Influence, causality and biophysical modeling," *NeuroImage*, vol. 58, no. 2, pp. 339–361, 2009.